


 Cite this: *RSC Adv.*, 2023, **13**, 12973

## First principles calculation to investigate the effect of Mn substitution on Cu site in $\text{CeCu}_{3-x}\text{Mn}_x\text{V}_4\text{O}_{12}$ ( $x = 0, 1, 2$ and $3$ ) system

F. F. Alharbi,<sup>a</sup> Shahid Mehmood,<sup>b</sup> Zahid Ali,<sup>b</sup> Salma Aman,<sup>c</sup> Rabia Yasmin Khosa,<sup>d</sup> Vladimir G. Kostishyn,<sup>e</sup> Sergei V. Trukhanov,<sup>ef</sup> M. I. Sayyed,<sup>g</sup> Daria I. Tishkevich<sup>id</sup><sup>ef</sup> and Alex V. Trukhanov<sup>id</sup><sup>ef</sup>

Structural, electronic, elastic and magnetic properties of  $\text{CeCu}_{3-x}\text{Mn}_x\text{V}_4\text{O}_{12}$  ( $x = 0, 1, 2$  and  $3$ ) system have been carried out through DFT using GGA, GGA+U and HF potential. The investigation of structural optimization reveals that lattice parameters of the understudy system is reliable with the reported results and are increasing with the Mn substitution due to their greater atomic radii as compare to Cu atom. Both the cohesive energy and the enthalpy show that  $\text{CeCu}_3\text{V}_4\text{O}_{12}$  is the most thermodynamically stable among these compounds. When Mn is replaced by Cu in these compounds, not only it become semi-metals, but the host compound also changes from non-magnetic to anti-ferromagnetic and their electrical resistance provides further credence to their electronic behavior. Mechanical stability, anisotropy, and ductility are all demonstrated through the elastic characteristics of these compounds. Due to anti-ferromagnetic ductile nature of the Mn base compounds, it is expected that the compounds in the system may use for spintronic application and in magnetic cloaking devices.

Received 13th January 2023

Accepted 13th April 2023

DOI: 10.1039/d3ra00263b

rsc.li/rsc-advances

### Introduction

Pulsed laser deposition (PLD) enables the hetero-epitaxial development of functional oxides, providing advantages for controlling their structural and physical properties. For instance, the critical temperature of superconducting cuprates is elevated by lateral compressive strain to a greater extent than by equivalent hydrostatic pressure.<sup>1</sup> Bismuth ferrites on  $\text{LaAlO}_3$  and  $\text{YAlO}_3$  (ref. 2–5) are two examples of films where epitaxial stress caused by lattice mismatches influences the ferroelectric characteristics or even changes the morpho-tropic phase. Similarly, doping can produce electronic or magnetic changes in certain perovskites manganates<sup>6</sup> or cobaltates.<sup>7</sup> Many magnetic thin films show strain-induced magnetic

anisotropy.<sup>8–10</sup> The occurrences above are primarily due to the interaction between the lattice changing and physical characteristics that determine the functionality of the oxides. In this investigation, we focus on a specific subset of perovskite oxides known as “quadruple perovskites,” which have the general formula  $\text{AA}'_3\text{B}_4\text{O}_{12}$ .  $\text{A}'\text{-B}$  inter-metallic charge transfer massive dielectric permittivity, oxygen reaction catalysis, negative thermal expansion and half-metallic<sup>11–18</sup> characteristics are just some of the many unusual qualities that have garnered them a lot of attention. The A site is often filled by alkali to rare-earth metals. In contrast, the  $\text{A}'$  site is normally taken by  $\text{Cu}^{2+}$  or  $\text{Mn}^{3+}$  elements.

The cation ratio between the 12-coordinate A cation and the 3-coordinate  $\text{A}'$  cation is 1:3. The sizeable octahedral tilting of  $\text{BO}_6$  stabilizes this A-site order. The quadruple perovskite oxides have a lattice parameter of 3.6–3.7 Å, making them quite dense. This could make sample preparation more challenging; conventional methods often include high-pressure synthesis at several giga pascal's.  $\text{CaCu}_3\text{Mn}_4\text{O}_{12}$  (ref. 19–22) which is semi-conducting, may be transformed into metal by replacing the Ca atoms with La or Bi atoms,<sup>10,11</sup> demonstrating the intriguing consequences seen for A-site replacements in these perovskites.

Charge disproportionation is also present in the isotropic combination  $\text{CaCu}_3\text{Fe}_4\text{O}_{12}$ . At the same time, the introduction of La or Bi into the A-site results in a markedly different pattern of inter-site charge transfer. The concentrated electrons in the A-site cations are accountable for their magnetic properties. In contrast, the oxygen atoms in the B-site cations play

<sup>a</sup>Department of Physics, College of Science, Princess Nourah Bint Abdulrahman University, P. O. Box 84428, Riyadh 11671, Saudi Arabia

<sup>b</sup>Center for Computational Materials Science, Department of Physics, University of Malakand, Chakdara, Dir (Lower), 18800 Pakistan

<sup>c</sup>Institute of Physics, Khwaja Fareed University of Engineering and Information Technology, Abu Dhabi Road, Rahim Yar Khan – 64200, Pakistan. E-mail: salma.physics.kfu@gmail.com

<sup>d</sup>University of Education, Lahore, Dera Ghazi Khan Campus, D. G. Khan, 32200, Pakistan

<sup>e</sup>Smart Sensors Laboratory, Department of Electronic Materials Technology, National University of Science and Technology MISiS, 119049 Moscow, Russia

<sup>f</sup>Laboratory of Magnetic Films Physics, Scientific-Practical Materials Research Centre of National Academy of Sciences of Belarus, 220072 Minsk, Belarus

<sup>g</sup>Department of Physics, Faculty of Science, Isra University, 1162 Amman, Jordan

a significant function in the material's electronic nature.<sup>9,12</sup> Perovskites arranged along the A-site with van der Waals valence at the B-sites exhibit intriguing behaviors. Paramagnetic and metallic properties are exhibited by Cu at A' and V at B sites, respectively. When V is substituted into the A'-site, the resulting change in the energy level of the Fermi level is distinct from combinations with Mn in the B-site or Fe.<sup>13</sup> Compounds in which A'-site is composed of both Mn and Cu and B-site is occupied by V are rare and less studied such as  $\text{CeCu}_{3-x}\text{Mn}_x\text{V}_4\text{O}_{12}$  ( $x = 0, 1, 2$  and  $3$ ) system.  $\text{CeCu}_3\text{V}_4\text{O}_{12}$  is studied by Kadyrova *et al.*<sup>23</sup> and reported their metallic paramagnetic nature.  $\text{CeCu}_{3-x}\text{Mn}_x\text{V}_4\text{O}_{12}$  ( $x = 0, 1, 2$  and  $3$ ) is only synthesized by the same group and only their structure properties were studied.<sup>24</sup>  $\text{CeMn}_3\text{V}_4\text{O}_{12}$  were studied by Kadyrova *et al.* experimentally<sup>25</sup> and theoretical<sup>26</sup> study demonstrates that the anti-ferromagnetism in this compound is due to Mn–O–Mn super exchange interaction.

The study of doping of elements on B-site in  $\text{AA}'_3\text{B}_4\text{O}_{12}$  compounds are available extensively<sup>27–29</sup> while very little study on the physical properties of doping at A'-site is reported such that transition from ferrimagnetic to anti-ferromagnetic in  $\text{LaCu}_3\text{Mn}_4\text{O}_{12}$  (ref. 30) and from ferromagnetic to anti-ferromagnetic in  $\text{RCu}_3\text{Mn}_4\text{O}_{12}$  ( $\text{R} = \text{Nd}$  and  $\text{Pr}$ )<sup>31</sup> and recently spin glass state is reported in  $\text{NdCu}_3\text{Mn}_4\text{O}_{12}$  by Mn substitutions at Cu site.<sup>32</sup> Keeping in view the effect of substitution at Cu site, the present study is performed to investigate the electronic structure in addition to elastic, thermoelectric and magnetic properties. The exchange correlation GGA, GGA with Hubbard  $U$  and HF are used within the WEIN2K package following the density functional theory (DFT) techniques for cutting-edge magnetic memory devices and spintronic technology.

## Results and discussion

### Structural analysis

The structural variables of the  $\text{CeCu}_{3-x}\text{Mn}_x\text{V}_4\text{O}_{12}$  ( $x = 0, 1, 2$  and  $3$ ) system were optimized in the realm of density functional theory (DFT) using GGA, GGA+ $U$ , and HF potentials with the assistance of experimental structure parameters.<sup>23–25</sup> The ground state energy of each unit cell shown in Fig. 1 against the ground state volume is estimated by appropriate the Birch–Murnaghan equation of state<sup>33</sup> and presented in Fig. 2. Table 1 lists the evaluated including the energy of the ground state ( $E_0$ ), the lattice constants ( $a_0$ ), the Cohesive energy ( $E_{\text{coh}}$ ) and the formation enthalpy ( $\Delta H$ ). The calculated  $a_0$  from the Table 1 for  $\text{CeCu}_3\text{V}_4\text{O}_{12}$  is  $7.327$ , for  $\text{CeCu}_2\text{MnV}_4\text{O}_{12}$  is  $7.358$ ,  $\text{CeCuMn}_2\text{V}_4\text{O}_{12}$   $7.431$  and for  $\text{CeCu}_3\text{V}_4\text{O}_{12}$  is  $7.462$  Å respectively. The results are consistent with experiments and theoretical results,<sup>23–26</sup> as shown by comparing the evaluated and reported  $a_0$  depicted in Fig. 3 and Table 1. The replacement of Mn on Cu site does not change the symmetry similarly in  $\text{LaCu}_{3-x}\text{Mn}_x\text{Mn}_4\text{O}_{12}$  ( $x = 1$  and  $2$ ) and  $\text{RCu}_{3-x}\text{Mn}_x\text{Mn}_4\text{O}_{12}$  ( $\text{R} = \text{Pr}$ ,  $\text{Nd}$  and ( $x = 1$  and  $2$ ))<sup>30,31</sup> and only leading to increasing the  $a_0$  of these compounds from  $\text{CeCu}_3\text{V}_4\text{O}_{12}$  to  $\text{CeMn}_3\text{V}_4\text{O}_{12}$ . The  $a_0$  of these compounds are growing due to greater ionic radius of Mn than Cu (Mn =  $0.097$  Å and Cu =  $0.087$  Å) as seen from the Fig. 2. The estimated ground state energies for  $\text{CeCu}_3\text{V}_4\text{O}_{12}$  is  $-37\ 034.439$  Ry,

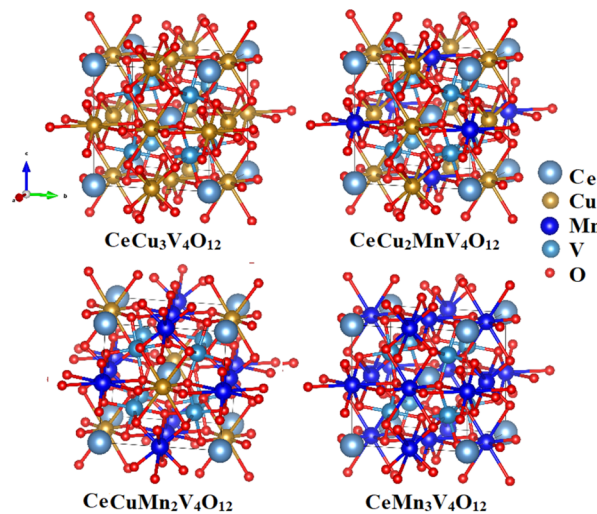


Fig. 1 Unit cell structure of the perovskites  $\text{CeCu}_{3-x}\text{Mn}_x\text{V}_4\text{O}_{12}$  ( $x = 0, 1, 2$  and  $3$ ).

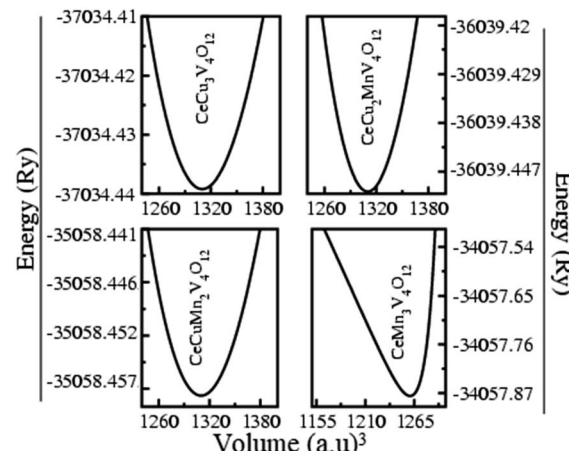


Fig. 2 Optimized ground state energies vs. volume of the perovskites  $\text{CeCu}_{3-x}\text{Mn}_x\text{V}_4\text{O}_{12}$  ( $x = 0, 1, 2$  and  $3$ ).

$\text{CeCu}_2\text{MnV}_4\text{O}_{12}$  is  $-36\ 039.447$  Ry,  $\text{CeCuMn}_2\text{V}_4\text{O}_{12}$  is  $-35\ 058.458$  and  $\text{CeCu}_3\text{V}_4\text{O}_{12}$  is  $-34\ 057.875$  respectively.

As shown in Table 1,  $E_{\text{coh}}$  and  $\Delta H$  are crucial stability factors that have been determined.<sup>26,34</sup> In a compound, the  $E_{\text{coh}}$  value is independent of the particle size and number of constituents. A larger value indicates a more firmly bound system because of electron nuclei interaction.  $E_{\text{coh}}$  and  $\Delta H$  for the system  $\text{CeCu}_{3-x}\text{Mn}_x\text{V}_4\text{O}_{12}$  ( $x = 0, 1, 2$  and  $3$ ) lie in the range of  $-41.612$  to  $-41.980$ ,  $-2.080$  to  $-2.099$  Ry,  $-39.80$  to  $-39.096$ ,  $-1.950$  to  $-1.954$  Ry,  $-37.501$  to  $-37.521$ ,  $-1.873$  to  $-1.876$  and  $-35.201$  to  $-35.931$  Ry and  $-1.746$  to  $-1.764$  Ry consequently.  $E_{\text{coh}}$  and  $\Delta H$  shows that the system  $\text{CeCu}_{3-x}\text{Mn}_x\text{V}_4\text{O}_{12}$  ( $x = 0, 1, 2$  and  $3$ ) is thermodynamic stable and the compound  $\text{CaCu}_3\text{V}_4\text{O}_{12}$  is show greater stability compare to all other compounds. Comparing the  $E_{\text{coh}}$  and  $\Delta H$  with the  $B_0$  for these compounds  $\text{CeCu}_{3-x}\text{Mn}_x\text{V}_4\text{O}_{12}$  ( $x = 0, 1, 2$  and  $3$ ) through Tables 1 and 2 show in Fig. 4. The figure discloses that all stability factors are



**Table 1** Estimated lattice constants ( $a_0$ ), ground state energy ( $E_0$ ), cohesive energy ( $E_{coh}$ ) and enthalpy ( $\Delta H$ ) of the  $\text{CeCu}_{3-x}\text{Mn}_x\text{V}_4\text{O}_{12}$  ( $x = 0, 1, 2$  and  $3$ ) compounds

Parameters	GGA	GGA+U	HF	EXP.	Others
<b>CeCu<sub>3</sub>V<sub>4</sub>O<sub>12</sub></b>					
$a_0$ (Å)	7.293	7.303	7.327		
$E_0$ (Ry)	−37 034.419	−37 034.071	−37 034.439		
$E_{coh}$ (Ry)	−41.960	−41.612	−41.980		
$\Delta H$ (Ry)	−2.098	−2.080	−2.099		
<b>CeCu<sub>2</sub>MnV<sub>4</sub>O<sub>12</sub></b>					
$a_0$ (Å)	7.321	7.341	7.358	7.360 (ref. 24)	
$E_0$ (Ry)	−36 039.443	−36 039.431	−36 039.447		
$E_{coh}$ (Ry)	−39.092	−39.080	−39.096		
$\Delta H$ (Ry)	−1.954	−1.950	−1.954		
<b>CeCuMn<sub>2</sub>V<sub>4</sub>O<sub>12</sub></b>					
$a_0$ (Å)	7.393	7.422	7.431	7.432 (ref. 24)	
$E_0$ (Ry)	−35 058.441	−35 058.402	−35 058.458		
$E_{coh}$ (Ry)	−37.521	−37.501	−37.546		
$\Delta H$ (Ry)	−1.875	−1.873	−1.876		
<b>CeMn<sub>3</sub>V<sub>4</sub>O<sub>12</sub></b>					
$a_0$ (Å)	7.411	7.436	7.462	7.480 (ref. 24), 7.469 (ref. 25)	7.46 (ref. 26)
$E_0$ (Ry)	−34 057.790	−34 056.515	−34 057.875		
$E_{coh}$ (Ry)	−35.291	−34.201	−35.931		
$\Delta H$ (Ry)	−1.760	−1.746	−1.764		

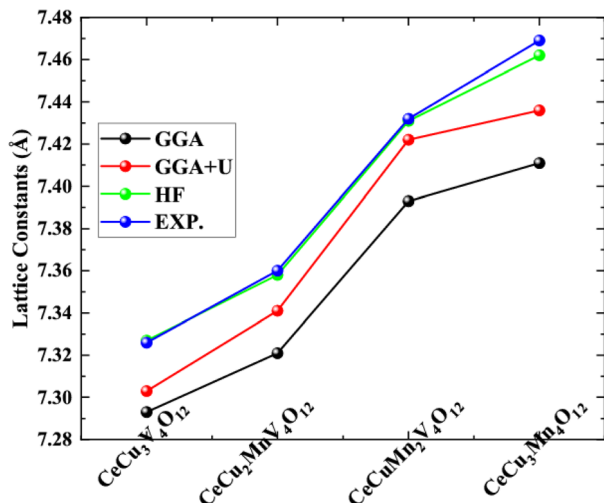


**Fig. 3** Correlation between the computed and observed lattice constant of perovskite structures  $\text{CeCu}_{3-x}\text{Mn}_x\text{V}_4\text{O}_{12}$  ( $x = 0, 1, 2$  and  $3$ ).

declining from Cu base compound to Mn containing compounds shows that the reduction in stability occurs from Cu to Mn and reveal the more stable nature of  $\text{CaCu}_3\text{V}_4\text{O}_{12}$  compound. Electronic charge density (ECD) in the (100) and (110) planes of  $\text{CeCu}_{3-x}\text{Mn}_x\text{V}_4\text{O}_{12}$  ( $x = 0, 1, 2$  and  $3$ ) are shown in Fig. 5 to shed light on the character of the chemical bonds between the atoms. By comparing the ECD via (100) and (110) planes, we can see that the Ce–O bond is ionic while the Mn/V–O bond is covalent. Fig. 5 shows that when one moves from Cu-based to Mn-containing compounds, the covalency between Mn/V–O raises and the ionic character of the Ce–O bond

decreases. However from the Pauling's method<sup>35,36</sup> using the formula % ionic character ( $P$ ) =  $(1 - e^{-1/4(E_{\text{Ce/Mn/V}} - E_{\text{O}})^2}(100\%))$ , where  $E_{\text{Ce/Mn/V}}$  and  $E_{\text{O}}$  is the electro-negativity of Ce/Mn/V and O atoms which suggest that Ce–O bonds are 75.24% and 73.96% ionic in nature and Mn–O and V–O bonds are respectively 40.95% and 44.09% covalent. Which further verifies the trend toward greater covalency and decreasing ionicity.

### Elastic properties

Specific boundary factors are connected to the materials functional applications and a material's elastic constants ( $C_{ij}$ ) show how it resists external stress. We are conscious of how structural materials react to applied pressure within their elastic range. In addition, a comprehensive knowledge of the elastic constants of the materials is essential for real-world applications. A solid's elastic and mechanical property are strongly linked to crystal symmetry orientations, mechanical stability, and anisotropic indices,<sup>37–39</sup> the WIEN2k software's integrated IRElast package is used to calculate the elastic parameters of the  $\text{CeCu}_{3-x}\text{Mn}_x\text{V}_4\text{O}_{12}$  ( $x = 0, 1, 2$  and  $3$ ) system described in Table 2. Mechanical factors; as shear modulus ( $G_H$ ), bulk modulus ( $B_0$ ), Reuss shear modulus ( $G_R$ ), Young's modulus ( $Y$ ), Poisson's ratio ( $\nu$ ), Paugh ratio ( $B_0/G_H$ ), shear constant ( $C'$ ), hardness parameters ( $H_V$ ), Cauchy pressure ( $C''$ ), Kleinman's parameter ( $\zeta$ ), anisotropic factor ( $A$ ), and Lame's constants ( $\lambda$  and  $\mu$ ) are examine using  $C_{ij}$ , listed in Table 2. All  $\text{CeCu}_{3-x}\text{Mn}_x\text{V}_4\text{O}_{12}$  ( $x = 0, 1, 2$  and  $3$ ) compounds exhibit mechanical stability as they meet the physical standards for the cubic phase compounds ( $C_{11} + 2C_{12} > 0$ ,  $C_{11} - C_{12} > 0$  and  $C_{44} > 0$ ) as specified in (ref. 40).

The value of  $G_R$ ,  $G_V$  and  $G_H$  from the Table 2 for  $\text{CeCu}_{3-x}\text{Mn}_x\text{V}_4\text{O}_{12}$  ( $x = 0, 1, 2$  and  $3$ ) compounds are in the range of



**Table 2** Calculated elastic moduli  $C_{ij}$ , ( $G_v$ ) Voigt's shear modulus, ( $G_R$ ) Reuss's shear modulus, ( $G_H$ ) Hill's shear modulus, ( $B_0$ ) bulk modulus, ( $B_0/G$ ) Pugh-ratio, ( $Y$ ) Young modulus, ( $H_v$ ) hardness parameters, ( $C''$ ) Cauchy-pressure, ( $A$ ) anisotropy constant, ( $\nu$ ) Poisson's ratio, ( $\zeta$ ) Kleinman parameter and ( $\lambda$  and  $\mu$ ) Lame's coefficients of the  $\text{CeCu}_{3-x}\text{Mn}_x\text{V}_4\text{O}_{12}$  ( $x = 0, 1, 2$  and  $3$ ) compounds

Mechanical parameters	$\text{CeCu}_3\text{V}_4\text{O}_{12}$	$\text{CeCu}_2\text{MnV}_4\text{O}_{12}$	$\text{CeCuMn}_2\text{V}_4\text{O}_{12}$	$\text{CeMn}_3\text{V}_4\text{O}_{12}$
$C_{11}$ (GPa)	408.763	397.489	389.314	385.781
$C_{12}$ (GPa)	168.540	158.764	150.198	145.567
$C_{44}$ (GPa)	131.506	125.696	121.344	117.632
$G_v$ (GPa)	126.948	123.163	120.560	118.609
$G_R$ (GPa)	126.698	123.084	120.553	118.609
$G_H$ (GPa)	126.823	123.123	120.556	118.615
$B_0$ (GPa)	248.614	238.336	230.132	225.633
$B_0/G$	1.960	1.935	1.908	1.902
$Y$ (GPa)	325.451	315.196	307.913	302.802
$H_v$ (Chen) (GPa)	12.46	12.42	12.48	12.40
$H_v$ (Tian) (GPa)	13.19	13.11	13.12	13.02
$H_v$ (Teter) (GPa)	19.15	18.59	18.20	17.91
$H_v$ (Miao) (GPa)	18.46	18.69	18.94	19.01
$H_v$ (Mazhnik) (GPa)	16.3	15.7	15.2	14.9
$C''$	37.033	33.064	29.197	27.930
$A$	1.094	1.053	1.016	0.979
$Y$	0.281	0.279	0.277	0.276
$\zeta$	0.696	0.676	0.657	0.643
$\lambda$	163.981	156.227	149.758	146.552
$\mu$	126.948	123.163	120.560	118.622

118.609 to 126.948, 118.609 to 126.698 and 118.615 to 126.832 GPa, respectively. This shows that  $\text{CeCu}_3\text{V}_4\text{O}_{12}$  has more opposition to plastic deformation than the  $\text{CeCu}_{3-x}\text{Mn}_x\text{V}_4\text{O}_{12}$  ( $x = 1, 2$  and  $3$ ). In response to an applied field,  $B_0$  quantifies the amount of material resistance.<sup>41,42</sup>  $B_0$  describes the increase in pressure that occurs with a negligible reduction in volume. In all cases, the calculated  $B_0$  value lies between 225.633 and 248.614 GPa. As shown in Fig. 4 from the EC and H, these results indicate that  $\text{CeCu}_3\text{V}_4\text{O}_{12}$  is the most resistant of the studied compounds to applying an external field.

The Pugh ratio explains why some materials are ductile while others are brittle. The material is ductile if the  $B_0/G_H$  ratio exceeds the critical threshold and brittle if it is less than 1.75.<sup>43</sup> These compounds are ductile, as their Pugh ratios are more

than the threshold value, coming in at 1.906, 1.935, 1.908, and 1.902, respectively.

The stiffness of the material is characterized by a higher value for the Young modulus ( $Y$ ). The elevated value of  $Y$  represents stiffness of the material and *vice versa*. The evaluated values of  $Y$  for these compounds vary from 302.802 to 325.451 GPa, demonstrating that all compounds show stiffness while  $\text{CeCu}_3\text{V}_4\text{O}_{12}$  is more rigid than others.

The hardness by different methods proposed by X. Chen *et al.*, N. Miao *et al.*, D. M. Teter, Y. Tian *et al.*, and E. Mazhnik *et al.*<sup>44–49</sup> and presented in Table 2. It can be observed from

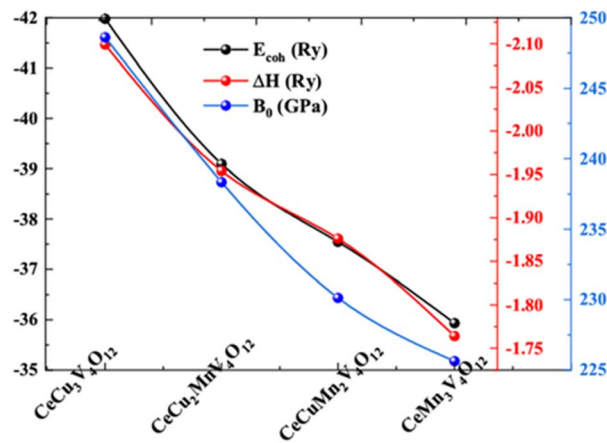


**Fig. 4** Correlation between cohesive energy, enthalpy, and bulk modulus of perovskite phases  $\text{CeCu}_{3-x}\text{Mn}_x\text{V}_4\text{O}_{12}$  ( $x = 0, 1, 2$  and  $3$ ).

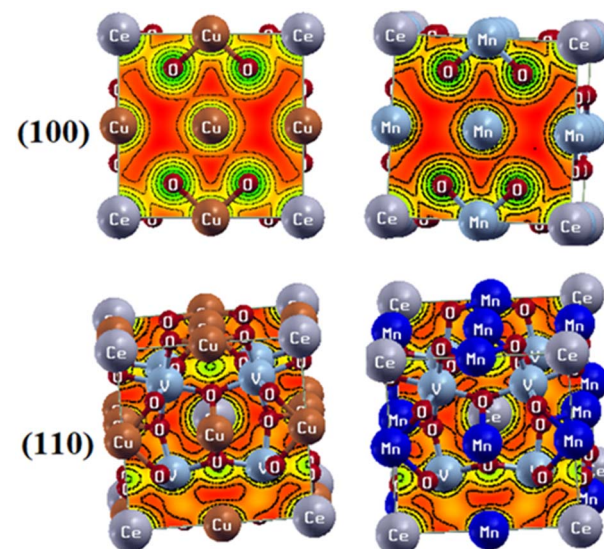


**Fig. 5** Chemical bonding in the perovskites  $\text{CeCu}_{3-x}\text{Mn}_x\text{V}_4\text{O}_{12}$  ( $x = 0$  and  $3$ ).



Table 2, the  $\text{CeCuMn}_2\text{V}_4\text{O}_{12}$  compound have maximum hardness value according to the Chen formalism and Tian, Miao and Mazhnik equations show that  $\text{CeCu}_3\text{V}_4\text{O}_{12}$  is hardest among the series. These compounds' proper hardness is exceptionally challenging in light of these findings. Mazhnik *et al.* have produced the most well-liked and widely accepted approach. The method uses the  $Y$  and  $v$  decides the hardness. According to Mazhnik approach the  $\text{CeCu}_3\text{V}_4\text{O}_{12}$  compound is the harder than the rest which is also indicated by the young modulus.

While investigating materials' ductile and brittle properties, the Cauchy pressure is also considered.<sup>50</sup> Materials with a positive value of Cauchy pressure are ductile, and those with a negative value are brittle. Pugh ratio estimates that all these compounds are in the ductile range, with values between 27.390 and 37.033 GPa.

The isotropic behavior of the material can be explained by its isotropic factor ( $A$ ).

Microcracks form as a result,<sup>51</sup> where  $A$  is equal to one for isotropic materials and 0 for anisotropic ones. All the compounds had  $A$  values between 0.979 and 1.094, indicating they are anisotropic.

The compressibility of a substance can be represented by Poisson's ratio ( $v$ ). These substances are calculated to be between 0.276 and 0.281 by measuring the shear and bulk moduli. Lower values in the range indicate unchanged in the symmetry, while higher values indicate whether volumetric changes have occurred. The calculated Poisson's ratios for the compounds under consideration, shown in Table 2, demonstrate volume fluctuation.

The Kleinman parameter ( $\zeta$ ) specifies the elasticity of the material's bonding. Using elastic coefficients, Harrison<sup>52</sup> developed a formula to determine the  $\zeta$ ; Kleinman's work demonstrates that  $\zeta = 0$  denotes bond bending, whereas  $= 1$  denotes bond stretching. Considering that the evaluated value for the complete set of compounds is between 0.643 and 0.696, we may infer that bond bending and stretching are possible in all combinations; this property is referred to ductility of these compounds. Bond bending overtakes bond stretching as the value approaches 1.

The values of  $Y$  and  $v$  determine Lame's constants ( $\mu$  and  $\lambda$ ). Changing the value of  $Y$  has a significant impact on both  $\mu$  and  $\lambda$ .<sup>53</sup> Since  $Y$  is low, lower are the values of  $\mu$  and  $\lambda$ . All the compounds considered are tough and stable, with Lame's constants falling in the range of 146.552–163.981 and 118.622–126.948. Overall, their elastic characteristics corroborate the compounds' ductile and anisotropic mechanical stability.

## Electronic properties

According to literature, the A'-site atom is the cause for the magnetic character; the B-site atom is the cause for the electronic nature in several quadruple perovskites that consist of binary magnetic elements. Adding a third magnetic element to the perovskite formula makes it very challenging to demonstrate the electrical and magnetic nature of the quadruple perovskite family. The total density of states (TDOS) plotted in Fig. 6 against the GGA, GGA+U, and HF potentials for the three

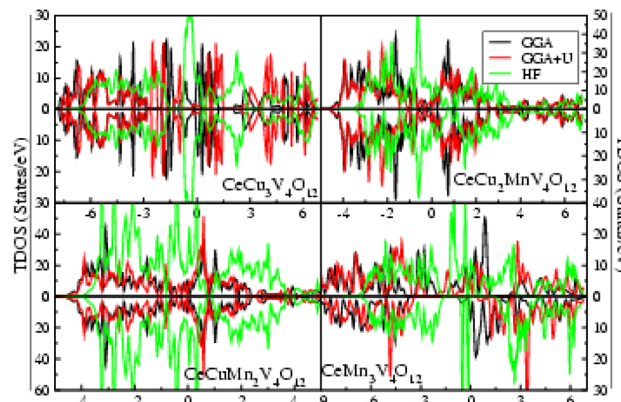


Fig. 6 Total density of states (TDOS) of the perovskites  $\text{CeCu}_{3-x}\text{Mn}_x\text{V}_4\text{O}_{12}$  ( $x = 0$  and 3).

magnetic perovskite sub-lattice systems helps clarify the ambiguity surrounding their relative metallicity. The figure discloses that all the compounds are metallic through GGA potential while GGA+U and HF gives metallic nature of  $\text{CeCu}_{3-x}\text{Mn}_x\text{V}_4\text{O}_{12}$  ( $x = 0, 1, 2$ ) except  $\text{CeCu}_3\text{Mn}_4\text{O}_{12}$  which is semi-metallic in nature. It has been reported, both theoretically and empirically, that  $\text{CeCu}_3\text{Mn}_4\text{O}_{12}$  (ref. 25 and 26) is semi-metallic wears experimentally it is reported that all others compounds are<sup>23,24</sup> metals, which reveal that the electrical properties of compounds change when Mn is completely replaced by Cu. The results obtained by GGA+U and HF are similar with slight difference such that all gives the same electronic character of the under-study compounds.

The electronic behavior of the  $\text{CeCu}_{3-x}\text{Mn}_x\text{V}_4\text{O}_{12}$  ( $x = 0, 1, 2$  and 3) compounds are also confirmed by calculating their band structure using HF potential and provided in Fig. 7. The figure disclose that the compounds  $\text{CeCu}_{3-x}\text{Mn}_x\text{V}_4\text{O}_{12}$  ( $x = 0, 1, 2$ ) are metallic such that energy bands are overlapping at the Fermi level while  $\text{CeCu}_3\text{Mn}_4\text{O}_{12}$  is semi-metallic due to overlapping of band in the up states and in spin down state no crossing over at the Fermi level occurs. Correspondingly the isotropic compounds show the same behavior such that the transition from metal to semiconductor occurs with the substitution of Ti and Fe at Mn site in  $\text{CaCu}_3\text{Mn}_4\text{O}_{12}$ ,  $\text{BiCu}_3\text{Mn}_4\text{O}_{12}$  and  $\text{LaCu}_3\text{Mn}_4\text{O}_{12}$ .<sup>54–56</sup>

The electrical resistivity for  $\text{CeCu}_{3-x}\text{Mn}_x\text{V}_4\text{O}_{12}$  ( $x = 0, 1, 2$  and 3) system is determined by BoltzTrap code<sup>57</sup> from 0 to 800 K temperature range and displayed in Fig. 8. The thermal velocity of electrons raise with rising temperature, leading to more collisions among free electrons and causing an increase in resistance, as shown in the graph for electrical resistivity. Electrical resistivity for  $\text{CeCu}_3\text{V}_4\text{O}_{12}$  is  $1.88 \Omega \text{ cm}$ , for  $\text{CeCu}_2\text{MnV}_2\text{O}_{12}$  is  $2.12 \Omega \text{ cm}$ ,  $\text{CeCuMn}_2\text{V}_2\text{O}_{12}$  is  $2.44 \Omega \text{ cm}$  and for  $\text{CeCu}_3\text{Mn}_4\text{O}_{12}$  is  $2.83 \Omega \text{ cm}$  at room temperature. The resistivity of  $\text{CeCu}_{3-x}\text{Mn}_x\text{V}_4\text{O}_{12}$  ( $x = 0, 1, 2$  and 3) are consistent with the experiment and with previous results.<sup>23–26</sup> Although the resistivity of  $\text{CeCu}_3\text{V}_4\text{O}_{12}$  is smaller and increases with Mn concentration. Similarly the resistivity of the  $\text{CaCu}_3\text{Mn}_4\text{O}_{12}$ ,  $\text{BiCu}_3\text{Mn}_4\text{O}_{12}$  and  $\text{LaCu}_3\text{Mn}_4\text{O}_{12}$  is also increases with Ti,<sup>54</sup> and with Fe doping.<sup>55,56</sup>



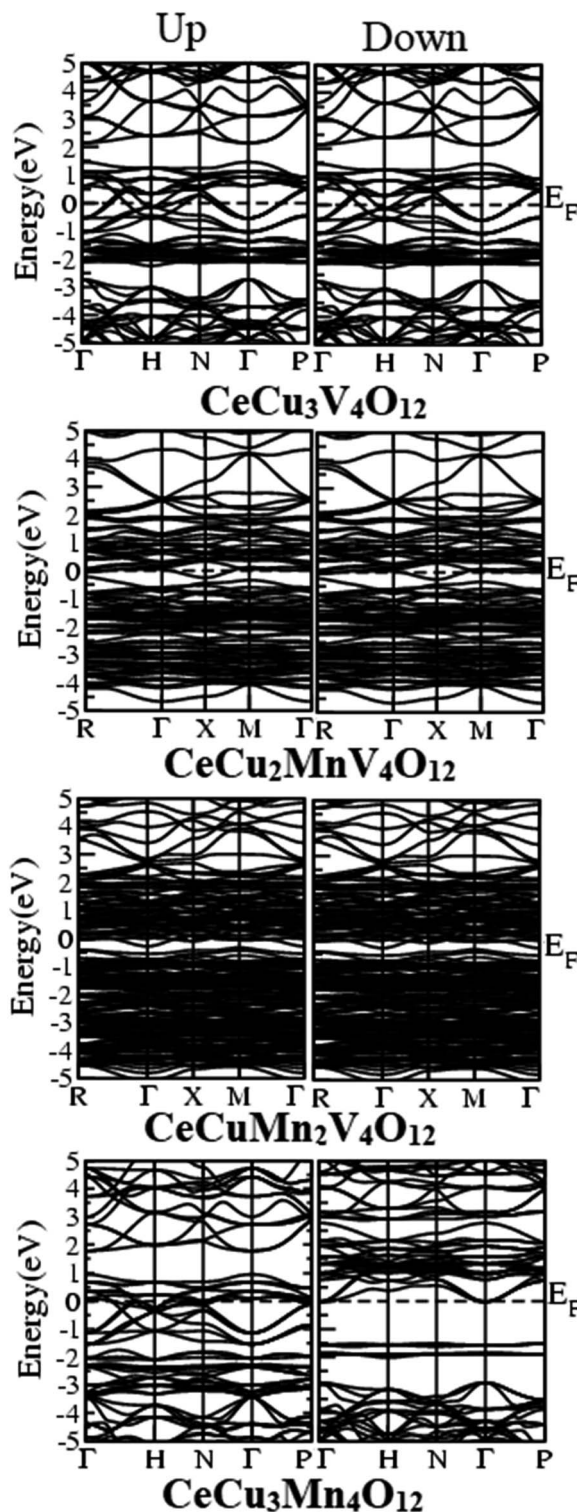


Fig. 7 Band structure of the perovskites  $\text{CeCu}_{3-x}\text{Mn}_x\text{V}_4\text{O}_{12}$  ( $x = 0, 1, 2$  and  $3$ ).

### Magnetic properties

Ground state magnetic energies are estimated for various magnetic configurations, including non-magnetic (NM), ferromagnetic (FM), and different types of anti-ferromagnetic (AFM).<sup>58,59</sup> This allows one to determine the stability of

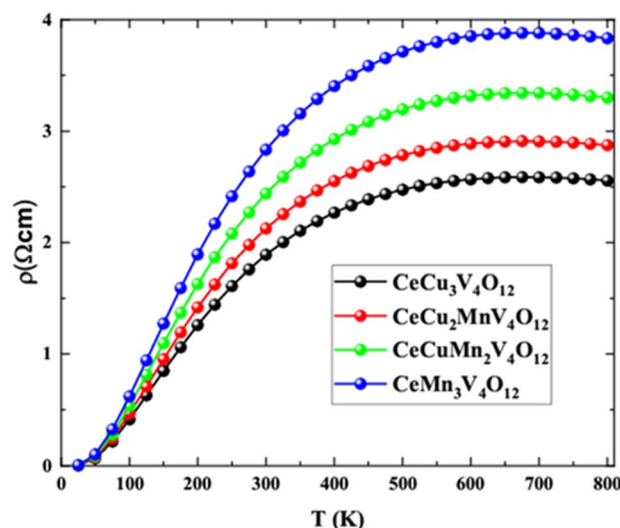


Fig. 8 Electrical resistivity of the perovskites  $\text{CeCu}_{3-x}\text{Mn}_x\text{V}_4\text{O}_{12}$  ( $x = 0, 1, 2$  and  $3$ ).

magnetic phase of  $\text{CeCu}_{3-x}\text{Mn}_x\text{V}_4\text{O}_{12}$  ( $x = 0, 1, 2$ , and  $3$ ) compounds. Fig. 9 depicts the energy of the magnetic ground state as a function of volume for these configurations. Fig. 9 shows  $\text{CeCu}_3\text{V}_4\text{O}_{12}$  and  $\text{CeCu}_{3-x}\text{Mn}_x\text{V}_4\text{O}_{12}$  ( $x = 1, 2$ , and  $3$ ) have reduced ground state energies due to their respective NM ordering and AFM nature, respectively. The findings regarding their magnetic properties are consistent with previous experimental and published data. Nevertheless, Mn doping causes a shift from the NM to the AFM phase<sup>24–26</sup> in the host  $\text{CeCu}_3\text{V}_4\text{O}_{12}$  compound.<sup>23</sup> Table 3 displays the estimated magnetic moments of the elements constituting these perovskites. Table 3 clearly shows that the magnetic moments of a copper atom are  $0.285$  and  $0.180$  and  $0.167\mu_B$ ; magnetic moments of Mn atom are  $4.073$ ,  $4.175$  and  $4.274\mu_B$ ; for V atom are  $0.052$ ,  $1.434$ ,  $1.347$  and  $1.254\mu_B$  respectively in  $\text{CeCu}_{3-x}\text{Mn}_x\text{V}_4\text{O}_{12}$  ( $x = 0, 1, 2$  and  $3$ ) compounds. The magnetic moment of Mn and V are reliable

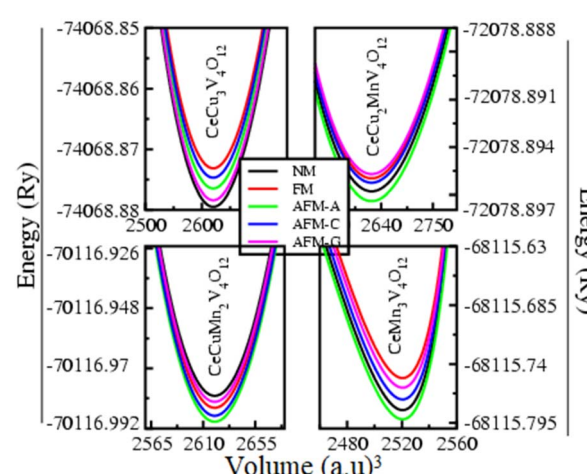
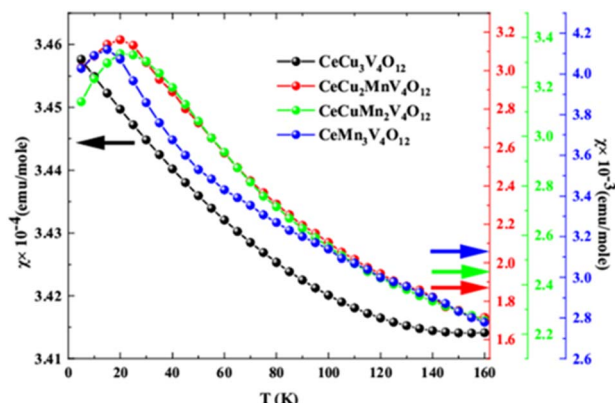


Fig. 9 Optimized ground state magnetic energy versus volume of the perovskites  $\text{CeCu}_{3-x}\text{Mn}_x\text{V}_4\text{O}_{12}$  ( $x = 0, 1, 2$  and  $3$ ).

Table 3 Magnetic moments for the  $\text{CeCu}_{3-x}\text{Mn}_x\text{V}_4\text{O}_{12}$  ( $B = 0, 1, 2$  and  $3$ )

Parameters	$\text{CeCu}_3\text{V}_4\text{O}_{12}$	$\text{CeCu}_2\text{MnV}_4\text{O}_{12}$	$\text{CeCuMn}_2\text{V}_4\text{O}_{12}$	$\text{CeMn}_3\text{V}_4\text{O}_{12}$
$\text{Cu} (\mu_B)$	0.285	0.180	0.167	—
$\text{Mn} (\mu_B)$	—	4.073	4.175	4.274
$\text{V} (\mu_B)$	0.052	1.432	1.347	1.254

Fig. 10 Magnetic susceptibility of the perovskites  $\text{CeCu}_{3-x}\text{Mn}_x\text{V}_4\text{O}_{12}$  ( $x = 0, 1, 2$  and  $3$ ).

with the other ( $4.27$  and  $1.25\mu_B$ )<sup>26</sup> observed results for  $\text{CeCu}_3\text{Mn}_4\text{O}_{12}$  which make the existing outcomes coherent and reasonable compare to others compounds. The magnetic moments of the Mn atom increases due to increase in its concentration and increases in the lattice constants of the system<sup>60</sup> and with the presence of the high Mn ion, same with the case in  $\text{RCu}_{3-x}\text{Mn}_x\text{Mn}_4\text{O}_{12}$  ( $x = 0, 1, 2$ ;  $\text{R} = \text{Pr}$  and  $\text{Nd}$ )<sup>31</sup>.

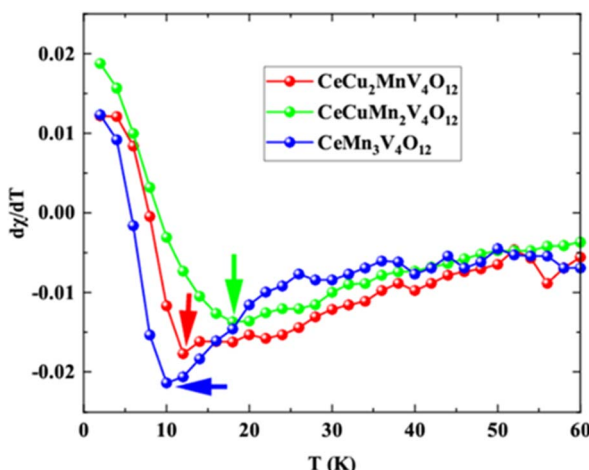
BoltzTraP code<sup>57</sup> is employed to find out the magnetic susceptibility and derivative of the magnetic susceptibility of  $\text{CeCu}_{3-x}\text{Mn}_x\text{V}_4\text{O}_{12}$  ( $x = 0, 1, 2$ , and  $3$ ) compounds. Magnetic susceptibilities calculated using the Curie–Weiss law<sup>61</sup> are depicted in Fig. 10.

The decreasing magnetic susceptibility with increasing temperature of  $\text{CeCu}_3\text{V}_4\text{O}_{12}$  indicates its NM nature. In contrast, the growing and subsequently decreasing magnetic susceptibility of  $\text{CeCu}_2\text{MnV}_4\text{O}_{12}$ ,  $\text{CeCuMn}_2\text{V}_4\text{O}_{12}$ ,  $\text{CeCu}_3\text{Mn}_4\text{O}_{12}$  indicates their AFM nature (as seen in the image). These compounds' magnetic susceptibility curves are incredibly comparable to the experimentally reported results for  $\text{CeCu}_3\text{Mn}_4\text{O}_{12}$ .<sup>25,26</sup> To determine the critical temperature ( $T_N$ ) the  $(d\chi/dT)$  is considered for the  $\text{CaCu}_{3-x}\text{Mn}_x\text{V}_4\text{O}_{12}$  ( $x = 1, 2$  and  $3$ ) system shown in Fig. 11. The anomalies for  $\text{CaCu}_{3-x}\text{Mn}_x\text{V}_4\text{O}_{12}$  ( $x = 1, 2$  and  $3$ ) system can be seen from Fig. 11 and Table 3. It is obvious that the abnormality happens at  $13$ ,  $18$  and  $10$  K correspondingly for  $\text{CaCu}_{3-x}\text{Mn}_x\text{V}_4\text{O}_{12}$  ( $x = 1, 2$  and  $3$ ). This work is reasonable and logical because the calculated TN of  $\text{CeCu}_3\text{Mn}_4\text{O}_{12}$  agrees well with the previously reported values ( $11.7$  and  $8$  K).<sup>24–26</sup> These compounds are essential for memory and spintronics because of their anti-ferromagnetic character, as demonstrated by the magnetic energy optimization and magnetic susceptibilities.<sup>62</sup> Aside from their practical uses, the absence of magnetic moments in these materials renders them unnoticeable to magnetic probes and insensible to instability in the magnetic field.<sup>63</sup> These materials' anti-ferromagnetic moments would affect their neighbors in spite of how closely the elements are arranged in the device. Still, they would also produce zero stray fields and eradicate the unintended magnetic crosstalk between neighboring devices.<sup>64</sup> Furthermore, the exchange between the dissimilar states of anti-ferromagnetic tends to be numerous times faster than ferromagnetic, making them very promising in increasing ultrafast and ultrahigh-density spy circuits.<sup>65</sup>

Thus, these materials are great for memory and spintronics since their AFM nature allows them for highly concentrated devices.

## Computational detail

The FP-LAPW approach in the DFT utilized in the WEIN2k package, was used to carry out the current investigation.<sup>66</sup> The GGA,<sup>67–69</sup> GGA+ $U$  and HF is employed to deal with the exchange and correlation.<sup>70</sup> The HF potential treat the correlated system (3d and 4f electron) very well especially in structure and electronic calculation,<sup>71,72</sup> due to the presence of 3d and 4f elements in the studied compounds hybrid functional are also used. The technique illustrated by Dudarev *et al.*<sup>73</sup> deal with the electronic correlation effect on Ce-f, Mn, Cu and V-d orbital's. According to the literature,<sup>26,74,75</sup> the effective  $U$  value chosen to be  $4$  eV per Ce,  $4$  eV per Mn,  $5$  eV per Cu and  $2$  eV per V respectively and the exact exchange  $\alpha$  for Ce is  $0.35$  eV is used throughout the calculation.

Fig. 11 The differential of magnetic susceptibility with respect to temperature in perovskite structures  $\text{CeCu}_{3-x}\text{Mn}_x\text{V}_4\text{O}_{12}$  ( $x = 0, 1, 2$  and  $3$ ).

The interstitial region is extended on a plane wave basis with  $K_{\max} = 6/R_{\text{MT}}$  as the cut-off value, the wave function is ubiquitous in the spherical harmonics contained within the muffin-tin spheres, which together make up the unit cell of the FPLAPW technique. For convergence to be guaranteed for less than one mRy a.u.<sup>-1</sup>, the Brillouin zone path employs a thousand K-point grids. Self-consistent field calculations<sup>76</sup> are used to compute the magnetic moments of the component elements in these compounds. Magnetic susceptibilities are evaluated using the BoltzTraP tool<sup>57</sup> and elastic properties are anticipated by IRElast package.<sup>77</sup>

## Conclusion

Structural, electronic and magneto-elastic properties of  $\text{CeCu}_{3-x}\text{Mn}_x\text{V}_4\text{O}_{12}$  ( $x = 0, 1, 2$  and  $3$ ) compounds have been studied in the domain of DFT. The examination of structural optimization reveals that the structural parameters of the  $\text{CaCu}_{3-x}\text{Mn}_x\text{V}_4\text{O}_{12}$  ( $x = 0, 1$  and  $2$ ) system are well consistent with experiments and are increases with Mn concentration. Electronic properties disclose the conductor nature of  $\text{CeCu}_{3-x}\text{Mn}_x\text{V}_4\text{O}_{12}$  ( $x = 0, 1$  and  $2$ ) while semi-metallic nature of  $\text{CeMn}_3\text{V}_4\text{O}_{12}$ . Beside this electrical resistivity also acknowledged their electronic nature. These elastic characteristics prove that these compounds are anisotropic, ductile as well as mechanically stable.  $\text{CeCu}_3\text{V}_4\text{O}_{12}$  is paramagnetic and  $\text{CeCu}_{3-x}\text{Mn}_x\text{V}_4\text{O}_{12}$  ( $x = 1, 2$  and  $3$ ) is anti-ferromagnetic determined from the spin dependent energy optimization. Their paramagnetic and anti-ferromagnetic nature is also confirmed from their magnetic susceptibility and the Néel temperature for  $\text{CeCu}_{3-x}\text{Mn}_x\text{V}_4\text{O}_{12}$  ( $x = 1, 2$  and  $3$ ) compounds are  $13, 18$  and  $10\text{ K}$  respectively estimated from the  $d\chi/dT$ . The anti-ferrimagnetic ductile nature of  $\text{CeCu}_{3-x}\text{Mn}_x\text{V}_4\text{O}_{12}$  ( $x = 1, 2$  and  $3$ ) compound identifies them promising materials for use in spintronics and magnetic cloaking.

## Data availability

The raw/processed data required to reproduce these findings cannot be shared at this time due to legal or ethical reasons.

## Conflicts of interest

The authors declare that they have no conflict of interest.

## Acknowledgements

Princess Nourah Bint Abdulrahman University Researchers Supporting Project number (PNURSP2023R55), Princess Nourah Bint Abdulrahman University, Riyadh, Saudi Arabia.

## References

- 1 J. P. Locquet, J. Perret, J. Fompeyrine, *et al.*, *Nature*, 1998, **394**, 453–456.
- 2 K. J. Choi, M. Biegalski, Y. L. Li, A. Sharan, *et al.*, *Science*, 2004, **306**, 1005–1009.
- 3 D. I. Tishkevich, A. I. Vorobjova, A. V. Trukhanov, *et al.*, *Solid State Phenom.*, 2020, **299**, 281–286.
- 4 D. Sando, A. Barthélémy and M. Bibes, *J. Phys.: Condens. Matter*, 2014, **26**, 473201.
- 5 A. V. Trukhanov, D. I. Tishkevich, S. V. Podgornaya, *et al.*, *Nanomaterials*, 2022, **12**, 868.
- 6 Y. Konishi, Z. Fang, M. Izumi, *et al.*, *J. Phys. Soc. Jpn.*, 1999, **68**, 3790–3793.
- 7 W. S. Choi, J.-H. Kwon, H. Jeen, *et al.*, *Nano Lett.*, 2012, **12**, 4966–4970.
- 8 A. Vorobjov, D. Tishkevich, D. Shimanovich, *et al.*, *RSC Adv.*, 2021, **11**, 3952.
- 9 H. Boschker, M. Mathews, E. P. Houwman, *et al.*, *Phys. Rev. B: Condens. Matter Mater. Phys.*, 2009, **79**, 214425.
- 10 A. Fedotov, V. Shendyukov, L. Tsybulskaya, *et al.*, *J. Alloys Compd.*, 2021, **887**, 161451.
- 11 A. A. Belik, *J. Chem. Soc., Dalton Trans.*, 2018, **47**, 3209–3217.
- 12 T. B. Adams, D. C. Sinclair and A. R. West, *Adv. Mater.*, 2002, **14**, 1321–1323.
- 13 Y. Long, N. Hayashi, T. Saito, *et al.*, *Nature*, 2009, **458**, 60–63.
- 14 Y. Long, T. Kawakami, W. Chen, *et al.*, *Chem. Mater.*, 2012, **24**, 2235–2239.
- 15 I. Yamada, S. Marukawa, M. Murakami, *et al.*, *Appl. Phys. Lett.*, 2014, **105**, 231906.
- 16 S. Yagi, I. Yamada, H. Tsukasaki, *et al.*, *Nat. Commun.*, 2015, **6**, 8249.
- 17 I. Yamada, H. Fujii, A. Takamatsu, *et al.*, *Adv. Mater.*, 2017, **29**, 1603004.
- 18 W. Chen, M. Mizumaki, H. Seki, *et al.*, *Nat. Commun.*, 2014, **5**, 3909.
- 19 D. I. Tishkevich, T. I. Zubov, A. L. Zhaludkevich, *et al.*, *Nanomaterials*, 2022, **12**, 1642.
- 20 Y. Lin, Y. B. Chen, T. Garret, *et al.*, *Appl. Phys. Lett.*, 2002, **81**, 631–633.
- 21 D. Tishkevich, A. Vorobjova, D. Shimanovich, *et al.*, *Nanomaterials*, 2021, **11**, 1775.
- 22 A. I. Vorobjova, D. I. Tishkevich, E. A. Outkina, *et al.*, *Nanomaterials*, 2022, **12**, 1344.
- 23 N. I. Kadyrova, Y. G. Zainulin, V. L. Volkov, *et al.*, *J. Inorg. Chem.*, 2008, **53**, 1542–1545.
- 24 N. I. Kadyrova, Y. G. Zainulin, N. V. Melnikova, *et al.*, *J. Inorg. Chem.*, 2018, **82**, 804–806.
- 25 N. I. Kadyrova, Y. G. Zainulin, A. P. Tyutyunnik, *et al.*, *Russ. J. Inorg. Chem.*, 2017, **62**, 103–110.
- 26 S. Mehmood, Z. Ali, I. Khan, *et al.*, *Mater. Chem. Phys.*, 2020, **254**, 123229.
- 27 S. Mehmood, Z. Ali, N. Alwadai, *et al.*, *J. Phys. Chem. Solids*, 2023, **174**, 111162.
- 28 S. Mehmood and Z. Ali, *J. Appl. Physiol.*, 2023, **129**, 76.
- 29 S. Mehmood, Z. Ali and I. Ahmad, *Mater. Chem. Phys.*, 2023, **295**, 127164.
- 30 A. Munoz, M. J. M. Lope, M. Retuerto, *et al.*, *J. Appl. Phys.*, 2008, **104**, 083911.
- 31 M. Retuerto, M. J. M. Lope, J. S. Benitez, *et al.*, *J. Appl. Phys.*, 2010, **108**, 083905.
- 32 Q. Zhang, Y. Breard and V. Hardy, *Inorg. Chem.*, 2022, **61**, 5792–5799.



33 F. Birch, *Phys. Rev.*, 1947, **71**, 809.

34 S. Mehmood, Z. Ali, I. Khan, *et al.*, *J. Electron. Mater.*, 2020, **49**, 3780–3790.

35 M. Lenglet, *Act. Passive Electron. Compon.*, 2004, **27**, 1–60.

36 Y. Slimani, N. A. Algarou, M. A. Almessiere, *et al.*, *Arabian J. Chem.*, 2021, **14**, 102992.

37 A. Bouhemadou, O. Boudrifa and N. Guechi, *Comput. Mater. Sci.*, 2014, **81**, 561–574.

38 A. Tasnim, Md. Mahamudujjaman, Md. A. Afzal, *et al.*, *Results Phys.*, 2023, **45**, 106236.

39 M. S. Hossain, N. Jahan, M. M. Hossain, *et al.*, *Mater. Today Commun.*, 2023, **34**, 105147.

40 L. Salik, A. Bouhemadou, K. Boudiaf, *et al.*, *J. Supercond. Novel Magn.*, 2020, **33**, 1091–1102.

41 M. H. K. Rubel, M. A. Hossain, M. K. Hossain, *et al.*, *Results Phys.*, 2022, **42**, 105977.

42 F. Khelfaoui, M. Ameri and D. Bensaid, *J. Supercond. Novel Magn.*, 2018, **31**, 3183–3192.

43 S. F. Pugh, *Philos. Mag.*, 1954, **45**, 823.

44 X. Q. Chen, H. Niu, D. Li and Y. Li, *Intermetallics*, 2011, **19**, 1275–1281.

45 Y. Tian, B. Xu and Z. Zhao, *Int. J. Refract. Hard Met.*, 2012, **33**, 93–106.

46 D. M. Teter, *MRS Bull.*, 1998, **23**, 22–27.

47 N. Miao, B. Sa, J. Zhou and Z. Sun, *Comput. Mater. Sci.*, 2011, **50**, 1559–1566.

48 E. Mazhnik and A. R. Oganov, *J. Appl. Phys.*, 2019, **126**, 125109.

49 R. Islam, M. M. Hossain, M. A. Ali, *et al.*, *RSC Adv.*, 2022, **12**, 32994.

50 D. G. Pettifor, *Mater. Sci. Technol.*, 1992, **8**, 345.

51 H. Fu, D. Li, F. Peng, *et al.*, *Comput. Mater. Sci.*, 2008, **44**, 774.

52 A. I. Vorobjova, D. L. Shimanovich, O. A. Sycheva, *et al.*, *Russ. Microelectron.*, 2019, **48**(2), 107–118.

53 L. Kleinman, *Phys. Rev.*, 1962, **128**, 2614.

54 H. Falcon, J. A. Alonso and J. S. Bentez, *J. Phys.: Condens. Matter*, 2006, **18**, 6841–6852.

55 P. Kayser, M. J. M. Lope, J. A. Alonso, *et al.*, *Solid State Chem.*, 2013, **204**, 78–85.

56 J. S. Bentez, M. RetuertoI, M. Jesus, *et al.*, *Z. Kristallogr.*, 2010, **225**, 201–208.

57 G. K. H. Madsen and D. J. Singh, *Comput. Phys. Commun.*, 2006, **175**, 67.

58 Q. Zhao, Y. Y. Yin, J. H. Dai, *et al.*, *Chin. Phys. B*, 2016, **25**, 020701.

59 A. L. Kozlovskiy, I. E. Kenzhina, M. V. Zdorovets, *et al.*, *Ceram. Int.*, 2019, **45**, 17236–17242.

60 J. Yang, Z. Xiao, Z. Li, *et al.*, *Computational Condensed Matter*, 2014, **1**, 51–57.

61 S. Mehmood, Z. Ali, I. Khan, *et al.*, *Mater. Chem. Phys.*, 2017, **196**, 222.

62 T. Jungwirth, X. Marti, P. Wadley, *et al.*, *Nat. Nanotechnol.*, 2016, **11**, 231–241.

63 J. Zelezny, P. Wadley, K. Olejnik, *et al.*, *Nat. Phys.*, 2018, **14**, 220–228.

64 S. Mehmood and Z. Ali, *Mater. Chem. Phys.*, 2022, **282**, 125915.

65 X. Li and J. Yang, *Natl. Sci. Rev.*, 2016, **3**, 365–381.

66 P. Blaha, K. Schwarz, F. Tran, *et al.*, *J. Chem. Phys.*, 2020, **152**, 07410.

67 A. M. Asiri, M. K. Shahzad, S. Hussain, *et al.*, *Helijon*, 2023, **9**, e14112.

68 M. K. Shahzad, S. T. Mujtaba, S. Hussain, *et al.*, *RSC Adv.*, 2022, **12**, 27517.

69 A. M. Asiri, M. K. Shahzad, S. Hussain, *et al.*, *Helijon*, 2023, **9**, e13687.

70 L. Wang, T. Maxisch and G. Ceder, *Phys. Rev. B: Condens. Matter Mater. Phys.*, 2006, **73**, 195107.

71 F. Tran, D. Koller and P. Blahaq, *Phys. Rev. B: Condens. Matter Mater. Phys.*, 2012, **86**, 134406.

72 A. S. Botana, F. Tran, V. Pardo, *et al.*, *Phys. Rev. B: Condens. Matter Mater. Phys.*, 2012, **85**, 235118.

73 S. Dudarev, G. Botton, S. Savrasov, *et al.*, *Phys. Rev. B: Condens. Matter Mater. Phys.*, 1998, **57**, 1505.

74 D. I. Tishkevich, A. I. Vorobjova, A. A. Bondaruk, *et al.*, *Nanomaterials*, 2022, **12**, 2382.

75 A. Shah, Z. Ali, S. Mehmood, *et al.*, *J. Electron. Mater.*, 2019, **49**, 1230.

76 J. C. Slater, *Phys. Rev.*, 1953, **91**, 528.

77 M. Jamal, M. Bilal, I. Ahmad, *et al.*, *J. Alloys Compd.*, 2018, **735**, 469.

